Automated quantification of choroidal neovascularization on Optical Coherence Tomography Angiography images

Kawther Taibouni, Yasmina Chenoune, Alexandra Miere, Donato Colantuono, Eric Souied, Eric Petit

Automated Quantification of Choroidal Neovascularization on Optical Coherence Tomography Angiography Images

Kawther Taibouni[a], Yasmina Chenoune[b,a], Alexandra Miere[a,c], Donato Colantuono[c], Eric Souied[c], Eric Petit[a]

[a] Université Paris-Est, LISSI (EA 3956), UPEC, F-94010, Vitry-sur-Seine, France

[b] ESME Sudria Research Lab, 40 rue du Docteur Roux, 75015 Paris, France

[c] Department of Ophthalmology, Centre Hospitalier Intercommunal de Créteil, 40, avenue de Verdun, 94000 Créteil, France

Email Addresses:

KT: kawther.taibouni@univ-paris-est.fr, YC: yasmina.chenoune@esme.fr, AM: alexandramiere@gmail.com, DC: colantuono.donato88@gmail.com, ES: esouied@hotmail.com, EP: petit@u-pec.fr

Corresponding author:

Kawther Taibouni
Université Paris-Est, LISSI (EA 3956), UPEC, F-94010, Vitry-sur-Seine, France

Financial or material support for the research and the work: none.

The authors have no proprietary interest in the materials used in this study.

Word count for text: 7086.

Word count for references: 1017.

Abstract

Objectives: To report the design of an automated quantification algorithm for choroidal neovascularization (CNV) in the context of neovascular age-related macular degeneration (AMD), based on Optical Coherence Tomography Angiography (OCTA) images.

Material and Methods: In this study, 54 patients (mean age 75.80 $\pm$ 14.29 years) with neovascular AMD (type 1 and type 2 CNV) were included retrospectively and separated into two groups (Group 1 – 24 images; Group 2- 30 images), according to the lesion topology. All patients underwent a 3x3 mm OCTA examination (AngioVue, Optovue, Freemont, California). The proposed algorithm is based on segmentation and enhancement methods including Frangi filter, Gabor wavelets and Fuzzy-C-Means Classification. Our results were compared to the manual quantifications given by the embedded quantification software "AngioAnalytics".

Results: Automated CNV segmentation and quantification of three neovascular AMD biomarkers: the total vascular area (TVA), the total area (TA) and the vascular density (VD) were possible in all cases. Automated versus manual quantification comparison revealed a statistically significant difference for TVA and VD measurements for both groups ($p = 0.00036$ for Group 1 TVA, $p < 0.0001$ for Group 1 VD and Group 2 TVA and VD). The difference in TA measurements was not significant in Group 2 ($p = 0.143$). Bland-Altman analysis revealed low inter-method bias for TA measurements and higher bias for TVA and VD.

Conclusion: This paper presents a method for segmenting and quantifying CNV that constitutes a valid option for clinicians. Complementary validations have to be carried out to compare our method's accuracy to "AngioAnalytics".

Keywords: Age-related Macular Degeneration; Choroidal Neovascularization; Optical Coherence Tomography Angiography; Vascular segmentation; Vessel enhancement filtering.

I. Introduction

Age-related macular degeneration (AMD) is the leading cause of irreversible visual loss in people 50 years or older, especially in developed countries [1], [2]. The advanced stage of macular degeneration is characterized by the presence of choroidal neovascularization (CNV). Neovascular AMD consists of abnormal or pathological blood vessels that originate from the choroid and grow into the avascular outer retina through the Bruch's membrane [3], [4]. Progression of CNV can result in subretinal hemorrhage, fluid exudation, lipid deposition, fibrosis, or a combination of these deleterious effects that result in photoreceptor damage and vision loss [1]–[4]. That is why the correct detection and precise location of the CNV plays a key role in further treatment decisions.

While the gold standard for the diagnosis of CNV in the context of AMD is considered to be fluorescein angiography (FA), indocyanine green angiography (ICGA) provides additional interesting information, particularly for type 1 CNV. However, these techniques are 2-dimensional (2D) and require intravenous dye injections [1].

Optical Coherence Tomography Angiography (OCTA) is a new non-invasive imaging technique able to overcome this limitation. It is a recent imaging technique that allows the visualization of retinal and choroidal microvasculature [5]. OCTA employs motion-contrast imaging to generate angiographic images by comparing the decorrelation signal between consecutive OCT B-scans taken at precisely the same cross-section to construct a blood flow map [6].

At diagnosis and during follow up, an accurate segmentation and quantification of CNV is required. To this day, CNVs are delineated manually, which is in itself a tedious and operator-dependent task. For these reasons, we developed an automatic image processing method to avoid this contribution of the clinician and to improve ophthalmologic diagnosis and patient follow up.

The segmentation of CNV is very challenging because OCTA images are degraded by projection and motion artifacts [5]–[7]. Moreover, as a consequence of physical principles of OCT, images are corrupted by speckle noise [8], that results in low contrast between CNV and image background. In addition, CNV lesions are very complex, with different shapes, sizes and locations and the flow visualization within these structures can significantly vary according to patients [1]. Only few works have been published for CNV segmentation from OCT-angiography images. Recently, Liu et al. [1] proposed an automated algorithm to detect choroidal neovascularization in outer retina *en face* angiograms from OCTA. The proposed algorithm was based on a context-aware saliency model for the vascular pattern recognition, which followed a preprocessing step to reduce projection artifacts from the outer retina. The CNV membrane mask was then generated by a post-processing step using nonlinear filtering, thresholding and morphological operations. The authors used this algorithm to quantify the CNV vascular area on 7 participants with neovascular AMD and compared their results to a CNV manual delineation with a good agreement. The main limit of this algorithm was the fact that it worked under the assumption that the CNV occupied a large portion of the image [9].

More recently, Xue at al. [9] proposed an automatic quantification method of the CNV total lesion area on outer retinal OCTA angiograms to overcome the limits of their previous saliency algorithm [1] that could not extract the CNV boundaries accurately. Their CNV segmentation method was based on an unsupervised and parallel machine learning technique named density cell-like P systems. The authors evaluated the CNV total lesion area segmentation on 22 scans of 22 patients with neovascular AMD and achieved an accuracy of 87%. Some inaccuracies of this algorithm were faced when noise pixels were bright and founded within the neovessels' neighborhood. In such cases, the density cell-like P systems method could not accurately discriminate vessel information from noise.

Nevertheless, there are several reviews of blood vessels segmentation and analysis techniques in the literature, usually applied to color fundus photography images [10]–[13]. Generally, vessel segmentation methods include two steps [14]. The first one is an enhancement of vascular structures mainly based on matched filter, Frangi filter or Gabor Wavelet filter [15]. The second step leads to the separation of tubular components of the image into vessel and non-vessel structures.

Following this scheme, our method is based on the enhancement of vessels located in the choroidal neovascularization lesion using the Frangi filter. Our database images are degraded by an intensive impulse noise, Frangi filter is thus the most suitable for the CNV enhancement because it is less sensitive to noise than matched filters and Gabor wavelets. In addition, it is faster and more efficient for emphasizing vessels of different sizes. Its principle is to detect geometrical structures in the image and to enhance them at different scales using Gaussian kernels [16]. As a second step, the differentiation between neovessels and non-neovessels structures is performed by Fuzzy-C-Means (FCM) classification.

Our purpose was to report a CNV automated segmentation and quantification algorithm and to compare these results with those generated by manual CNV segmentation and quantification using the embedded algorithm. Our method was designed so as to segment different shapes, sizes and locations of CNV and to preserve details according to the topology in order to obtain a correct quantification of the CNV biomarkers on a larger cohort (54 participants). The previous works on CNV segmentation only dealt with the total area or the CNV vascular area quantification on small cohorts (7 participants [1] and 22 participants [9]) whereas our method have been designed to estimate three biomarkers of neovascular AMD; the CNV vascular area, the CNV total area and the CNV vascular density. These are the three biomarkers currently used by clinicians for the patients' follow up and in clinical research.

II. Materials and Methods

Inclusion and exclusion criteria

This retrospective monocentric case series included consecutive patients with active type 1 and type 2 CNV secondary to neovascular AMD, previously treated and treatment-naive, presenting at the University Eye Clinic of Créteil between October 2015 and April 2018. This study was performed in accordance with the Declaration of Helsinki and current French legislation and with approval of our local ethics committee.

Eligibility criteria were a diagnosis of CNV based on the FA international AMD classification [17]. Exclusion criteria consisted of other forms of neovascular AMD, such as type 3 neovascularization, idiopathic polypoidal choroidal vasculopathy, ocular diseases associated with pigment epithelial detachments, adult onset foveomacular vitelliform dystrophy, history of highly myopic CNV or pathological myopia, as well as a history of inherited macular dystrophies.

All the patients underwent a 3x3 mm OCTA examination (AngioVue, Optovue, Freemont, CA). The OCTA flow images size was of 304 x 304 with a pixel size of 9.87 x 9.87 μm. This definition allowed an accurate visualization of small vessels. The outer retinal slab with projection artifact removal was extracted when the image quality assessed using the Strength Signal Index SSI was greater than or equal to 6 (SSI $\geq$ 6) and manual editing of the outer retinal segmentation was performed if the software segmentation was not satisfying. Manual CNV delineation and quantification was obtained for all patients by an expert reader (AM).

Included patients were further separated into two groups according to the CNV's topology on the images. Group 1 consisted of densely packed high flow networks, with no distinguishable branching (Figure 1, Panel A). Group 2 consisted of a high flow neovascular network with distinguishable individual branching pattern (Figure 1, Panel B). A distinct algorithm was developed for each group. Two common steps preceded each algorithm: firstly, contrast enhancement in addition to a classic median filtering was employed, so as to separate the lesions from noise and to clearly distinguish the CNV contours; secondly, clinician interaction was solicited to select one or more markers on the flow image to indicate the lesion location. The proposed

method was compared with manual delineation of the CNV and quantitative analysis with the embedded software (AngioAnalytics).

Proposed segmentation method for Group 2

Image filtering reduces the small details that can be in our case thin vessels or connections between vessels. This problem led to perform preprocessing on two paths. One aims to reduce the image noise while preserving the neovascular fine details. The other processing path ensures the isolation of the CNV lesion from noise while ignoring the neovascular network details. The input flow image is thus preprocessed twice as indicated in the algorithm overview of Figure 2.

Vessel Enhancement

The CNV enhancement was performed using Frangi filter that heightens the lesion based on information on vessel size. In fact, the Frangi filter is a multiscale vessel enhancement filter that considers the eigenvalue analysis of the image Hessian matrix to determine a vesselness measure function [16]. The latter ensures the vessels enhancement at different scales σ which correspond to the vessels thickness (size) using the image second derivative and a Gaussian kernel [14], [18]. Because of the variation in the shape and size of the CNV between patients, several experiments were performed to define the σ variation range that was ultimately defined as $\sigma = \{1, 2, 3\}$. Figure 2 illustrates the application of the Frangi filter for the two processing paths mentioned previously.

Segmentation

As mentioned earlier, preprocessing and vessel enhancement are performed on two paths. The resulting image of the first path is used to define a marker image to reconstruct the CNV lesion using the resulting mask image of the second path. The marker image is first defined using the Gabor Wavelets and the entropy maximization thresholding. Many works have demonstrated the effectiveness of using Gabor wavelets to segment the retinal vascular network [19]–[21] since they succeed in emphasizing directional components and can be tuned to capture certain frequencies. In our proposed method, Gabor wavelets are tuned to ensure the homogenization of the neovascular zone by connecting the vessels within the lesion in order to construct a

connected region of interest (ROI). Precisely, the image is filtered by twelve wavelets using a wavelength equal to 5 and twelve different orientations from 0° to 330° with a +30° variation between the wavelets' orientations. A thresholding based on the maximization of the image entropy is applied to the previously filtered image to extract the neovascular ROI using the manually selected markers (clinician interaction) [22], [23]. Once the marker and the mask images are defined, a morphological reconstruction is performed to precisely reconstruct the CNV lesion.

The reconstructed CNV may contain some noise or background pixels. Consequently, the separation of the reconstructed pixels into neovascular pixels and background pixels is necessary. Several experimentations were performed using different thresholding techniques such as Otsu, Adaptive and Global thresholding. Hysteresis thresholding by Fuzzy C-means classification was the only thresholding method that allowed a good separation of CNV pixels from the background for all of the studied cases. We thus chose to apply the Fuzzy-C-Means classification for separating the pixels on images into three clusters: CNV lesion, image background and a fuzzy cluster. This classification result made it possible to calculate two thresholds (a high threshold and a low threshold) for the CNV binarization by hysteresis thresholding [24]. Figure 2 illustrates in detail the different segmentation steps for this group of flow images.

Proposed segmentation method for Group 1

Since the OCTA flow images in this group are less complex than the previous ones, preprocessing is performed in a single path using a classic median filtering. In addition, there is no need to vessel enhancement because the CNV appears as a densely packed region. Segmentation is therefore processed in three main steps: pixel classification, hysteresis thresholding and CNV region extraction. The two first steps are performed similarly to the previous segmentation algorithm. Then, the neovascular region is extracted using the manually selected markers. Figure 3 gives an overview of the developed segmentation and quantification algorithm for Group 1 flow images.

Quantification

The resulting segmentations were used to automatically quantify three biomarkers of neovascular AMD, namely the total vascular area (TVA), the total Area (TA), and the vascular density (VD) which is the ratio between the TVA and the TA. However, to obtain an exact quantification of the TVA and TA, it is necessary to improve the resulting segmentations in order to recover the neovascular pixels removed during the hysteresis thresholding. In fact, the last binarized image is used to reconstruct a well-defined neovascular ROI by several morphological closings. For Group 2 segmentations, an oriented straight structuring element is used, while a circular structuring element with an adequate radius is applied for Group 1 segmentations. The TA is the area of this well-defined ROI.

This well-defined ROI is also used to delineate the reconstructed CNV to estimate the TVA for the Group 2 segmentations, where the surface of the delineated neovessels is the surface of the lesion. On the other hand, the TVA is measured directly from the Group 1 resulting segmentation to finally estimate the vascular density.

Statistical analysis

Statistical analysis is performed using XLSTAT, a data analysis and statistical solution for Microsoft Excel (XLSTAT 2016, Addinsoft, Paris, France) and included Student's t-test, linear regression and Bland-Altman analysis. T-test is used to compare the mean values of the automatic estimated biomarkers versus the manual estimated biomarkers. Linear regression is used to study the correlation between the automatic and the manual measurements. As regards Bland and Altman analysis, it is performed to evaluate the agreement between our developed algorithms and the manual delineation obtained with AngioAnalytics. For each biomarker, the means of the measurements are plotted along the X axis and the differences between the measures of the methods along the Y axis. The measurements are considered to be in agreement when most of the plots are within the agreement limits (mean +/- 2 SD). For all findings, the chosen level of statistical significance was $\alpha < 0.05$.

III. Results

Fifty-four eyes of 54 patients were included in this study, ranging from 26 to 91 years (mean age: 75.80 years ± 14.29 SD), with neovascular AMD. The overall studied population was divided into Group 1 -consisting of 24 eyes- and Group 2 -consisting of 30 eyes-. We proposed a different segmentation algorithm for each group. MATLAB R2017a (The MathWorks, Inc., Natick, Massachusetts, United States) was used for the software implementation.

Automated versus manual quantitative analysis using AngioAnalytics is summarized in Table 1. The mean value of the measured total vascular area (TVA) for Group 1 is of 0.402 ± 0.380 mm^2 using the automated algorithm, against an average value of 0.494 ± 0.469 mm^2 estimated by AngioAnalytics. Similarly, the TVA average value measured automatically for Group 2 is of 0.400 ± 0.395 mm^2 against an average of 0.556 ± 0.568 mm^2 given by AngioAnalytics.

The total area (TA) automatic measurements are closer to those of AngioAnalytics than TVA measurements. Group 1 automatic mean value is of 0.592 ± 0.564 mm^2, while the average value of AngioAnalytics measurements is of 0.631 ± 0.591 mm^2. Group 2 automatic TA mean value is of 0.791 ± 0.740 mm^2, against an average value of 0.815 ± 0.761 mm^2 obtained with AngioAnalytics.

For the vascular density (VD) measurements, the automatic mean value of Group 1 is of 70.3% ± 11.0% against an average of 77.9% ± 9.1% given by AngioAnalytics. The Group 2 automatic VD average value is of 52.6% ± 10.2% against the AngioAnalytics mean value of 69.4% ± 10.4%.

There was a statistically significant difference between the manual and the automated quantification concerning TVA and VD (Student's t-test, Group 1: $p = 0.00036$ for TVA, $p < 0.0001$ for VD; Group 2: $p < 0.0001$ for both TVA and VD). However, the difference between the two quantification methods for TA was non-significant in Group 2, with $p = 0.143$ (Student's t-test).

As regards the Bland and Altman analysis, biases of the inter-methods agreement are summarized in Table 2. Group 1 TVA bias was of -0.092 ± 0.107 mm^2 (95% confidence interval (CI) ranging from -0.137 to -0.046 mm^2), while Group 2 bias was higher estimated of -0.156 ± 0.189 mm^2 (95% CI ranging from -0.227 to -0.085 mm^2).

For the total area (TA), biases were very weak for both groups, -0.039 ± 0.066 *mm²* (95% CI -0.067 to 0.011 mm²) for Group 1 and -0.023 ± 0.085 *mm²* (95% CI -0.055 to 0.008 mm²) for Group 2. In contrast, biases for the vascular density (VD) were high for both groups, -7.7 ± 5.6 % for Group 1 (95% CI -10.0 % to -5.3%) and -16.8 ± 5.9 % (95% CI -19.0 % to -14.6%) for Group 2.

Figure 4 illustrates the Bland-Altman plots, where 95.83 % of the TVA plots and 91.67 % of the TA and VD plots are within the agreement limits for Group 1. Similarly, 96.67 % of the TVA and VD plots and 93.33% of the TA plots are in the Bland-Altman agreement zone for Group 2.

Correlation coefficients (CC) estimated by linear regression (figure 5) were high for TVA and TA measurements for both groups (Group 1: TVA CC = 0.989, TA CC = 0.994; Group 2: TVA CC = 0.987, TA CC = 0.994). However, VD measurements showed lower coefficients for both groups (Group 1: VD CC = 0.859; Group 2: VD CC = 0.836).

Segmentation workflow for Group 2 automated algorithm is illustrated in figure 6, where panel A illustrates a high flow neovascular network (CNV) visualized on the outer retinal slab of OCTA, on which two markers were selected by the clinician. Preprocessing of the 1st path well isolated the neovascular network from the impulse noise although some neovascular fine details have been filtered (figure 6, panel B). On the other hand, the 2nd path preprocessing slightly reduced the image noise but preserved all the neovascular details (figure 6, panel C). Applying Frangi filtering on these two preprocessed images further isolates the neovascular network and enhances all thin and wide neovessels (figure 6, respectively panels D and E). In figure 6, panel F, one can see that Gabor filtering well homogenizes the neovascular surface, which once binarized by entropy maximization (figure 6, panel G) allowed the extraction of the neovascular ROI using the initially selected markers (figure 6, panel H). The CNV is reconstructed in the figure 6, panel I using the images of figure 6, panel E and H as mask and marker images. The CNV is binarized in the Figure 6, panel J by hysteresis thresholding based on the FCM classification of figure 6, panel I. The image (figure 6, panel K) illustrates the creation of the well-defined ROI using morphological closing on the image of figure 6, panel J. Finally, figure 6, panel L displays the resulting segmentation where the CNV is well-defined and delineated.

The workflow of the Group 1 segmentation automated algorithm is illustrated in figure 7 where the 1st image (figure 7, panel A) displays the original OCTA flow image on which one marker was manually selected by

the clinician. The resulting image of the preprocessing is illustrated in figure 7, panel B and the resulting image of the hysteresis thresholding in figure 7, panel C. Then, the CNV is extracted using the previously defined marker and shown on figure 7, panel D, while the creation of the neovascular ROI using morphological closing is shown on figure 7, panel E. Figure 7, panel F displays the final segmentation result where the CNV is well segmented and delimited.

Figure 8 illustrates the comparison between automatic and manual segmentations where the flow images (panels A1 and A2) are corrupted by movement artifacts (white line artifacts) connected to the CNV. Our segmentation of the total area on these images (see panels B1 and B2) agrees with the expert manual delineation of the CNV total area in both cases (respectively panels C1 and C2). However, the main difference between the automatic segmentation and the AngioVue segmentation occurs in the size of the neovessels that are thickened by AngioVue algorithm, as we can see on figures C1 and C2. It seems to include a larger vascular area than our algorithm compared to the original images A1 and A2. Both segmentations B1 and C1 included some artifacts to the CNV segmentation (on the top right for B1, inside the CNV area for C1). Moreover, our automatic segmentation, showed in B2, filtered some neovessels in the bottom right of the CNV while AngioVue segmentation in C2 included some noise within the lesion.

Figure 9 represents the performance evaluation of our algorithms on regards to the segmentation time. All experiments are conducted on a computer with an Intel® Core™ i7-8650U CPU @ 1.90 GHz 2.11 GHz. According to the segmentation curves below, our two proposed algorithms take linear time or O(n) time. Linear time is the best possible time complexity for our proposed methodology, where the two algorithms have to sequentially read the entire OCTA images. Precisely, the clinician should load at each time an OCTA input image and then select one or more CNV markers.

IV. Discussion

OCT-Angiography is a recent non-invasive imaging technique for visualizing retinal and choroidal physiological and pathological vascularization. In this study, we proposed two choroidal neovascularization segmentation and quantification algorithms for two different groups of OCTA flow images, in order to quantify currently-used biomarkers of neovascular AMD by the same algorithm for each group. The two

algorithms were mainly based on three steps: preprocessing, segmentation and quantification. However, the Group 2, in which the individual branching of the neovascular network was distinguishable, flow images analysis required an additional vessel enhancement step on two processing paths in order to preserve the network vascular pattern details and obtain precise segmentation and quantification.

We tested the two algorithms on 54 OCTA flow images of 54 patients with type 1 and 2 CNV (24 flow images in Group 1 and 30 flow images in Group 2). Furthermore, we showed that our algorithms were able to extract and quantify different shapes and types of CNV. When comparing the biomarkers (TVA, TA and VD) using our proposed methods, to the tool embedded in the AngioVue Software "AngioAnalytics" (after the manual delineation of the CNV by one expert), the correlation coefficients by linear regression were very high for TVA and TA measurements of both groups (Group 1: TVA CC = 0.989, TA CC = 0.994; Group 2: TVA CC = 0.987, TA CC = 0.994) and lower for VD measurements (Group 1: VD CC = 0.859; Group 2: VD CC = 0.836).

We reported in table 2 the Bland and Altman biases for the inter-methods agreement for each biomarker. Biases were very weak for TA measurements of both groups: -0.039 ± 0.066 mm^2 (95% CI -0.067 to 0.011 mm^2) for Group 1 and -0.023 ± 0.085 mm^2 (95% CI -0.055 to 0.008 mm^2) for Group 2. Thus, our automatic measurements of the total area agree well with the expert manual delineations. In addition, the student's t-test showed that the difference between the two quantification methods for TA was non-significant in Group 2, with p = 0.143. The segmentations we propose can therefore be a good alternative to the manual delineations that are the only ground-truth we have from the experts.

However, biases for the total vascular area (TVA) measurements were higher than TA biases for both groups. Group 1 bias was -0.092 ± 0.107 mm^2 (95% CI ranging from -0.137 to -0.046 mm^2) and -0.156 ± 0.189 mm^2 (95% CI ranging from -0.227 to -0.085 mm^2) for Group 2; which means that AngioAnalytics overestimates the neovascular area. This may explain the difference between our measurements of vascular density (VD) and AngioAnalytics measurements that are reported in biases of table 2 (Group 1 VD: -7.7 ± 5.6 % (95% CI -10.0 % to -5.3%); Group 2 VD: -16.8 ± 5.9 % (95% CI -19.0 % to -14.6%)). In fact, AngioAnalytics segmentation of the CNV could include some noisy pixels as neovascular pixels and thus overestimates the

total vascular area due to a lack of preprocessing. Conversely, our method could remove some neovascular pixels due to the preprocessing step and thus underestimates the total vascular area. Additional studies should be done to identify which of the two segmentations is the most accurate.

Due to the variability in CNV pattern and the physical principles of OCTA, some images of the studied series were quite complex and very noisy. As mentioned before, shape, location and size of the lesions vary from one image to another. Precisely, images may include localized or more extended artifacts, in particular, movement artifacts (white line artifacts) that can be considered as tubular structures and segmented with the CNV. The markers' selection by the expert was very effective against the different artifacts present on the flow images and allowed their exclusion from the resulting segmentations. However, this problem remained on few images where white line artifacts were segmented as vascular components, as we can see it on figure 9 – panel B. Improvements of our algorithms can be considered to face this limit. Furthermore, the quantification performed in this study is based on two-dimensional flow images, advanced studies on three-dimensional data can so be performed to obtain volumetric measurements.

Finally, it is notable to highlight our main contributions in relation to the existing few works [1] and [9]. In the present study, a larger number of OCTA flow images was used and was separated according to the CNV topology into two groups, in order to preserve vascular details and have a correct quantification of the CNV. Three biomarkers of neovascular AMD were quantified by the same algorithm for each group. In addition, the results were compared to those obtained from AngioAnalytics which is the embedded algorithm, widely used in the current clinical routine.

The performances of our proposed segmentation algorithms for the total area segmentation are compared in Table 3 with the saliency method and the DEC P systems proposed in [1] and [9] respectively. In summary, our methods achieved better accuracy of 87.5 %, especially the Group 2 algorithm where accuracy was of 88.17 % with respect to Jaccard Coefficient.

CNV automatic quantification on OCT-Angiography devices is strongly needed in clinical research and practice. That is why recent works have extensively focused on the role of the CNV quantification in the follow-up of neovascular AMD patients. Amoroso et al [25] have evaluated the reproducibility and the

interuser agreement of the CNV lesion size manual measurements on OCTA using the measuring tool embedded in the AngioVue software. Although this work has shown that these measurements are reproducible, it has also revealed the importance of automatic CNV segmentation and quantification to avoid manual implication of clinicians for CNV segmentation.

Miere et al [26] have studied the changes of the CNV after anti-VEGF therapy by quantifying the CNV size at baseline and at three monthly follow-up visits. Their report showed that treatment naïve and treated eyes with CNV secondary to neovascular AMD responded differently to anti-VEGF therapy. Coscas et al [27] have analyzed quantitative OCTA biomarkers, such as blood flow area, fractal dimension and vessel density, for neovascular AMD patients under-treatment and in remission. Through this study, the authors have shown that studying these biomarkers on OCTA could become a valuable technique in assessing the CNV response to anti-VEGF agents and helping clinicians to develop personalized treatment and follow-up cycles.

Other works on the assessment of anti-VEGF treatment for CNV on OCTA have used the AngioVue software to quantify the CNV area and the flow area using the embedded algorithm "AngioAnalytics" according to the manual delineation of two qualified technicians [28]. In addition, Xu et al [29] have recently analyzed the long-term growth patterns of type 1 CNV in eyes with AMD receiving anti-VEGF therapy, based on the CNV manual segmentation on OCTA images and the OCTA area measurements. Therefore, an automated quantification method may be useful and time-saving instrument for clinicians in assessing treatment-response and natural history of CNV complicating neovascular AMD.

Other retinal vessel segmentation methods have been proposed in the literature and could be adapted to the CNV segmentation and quantification in further studies. Oloumi et al. [30] have proposed a novel method for the detection, segmentation, tracking and measurement of the thickest venular branch width in the retina (The major temporal arcade) on retinal fundus images. The proposed method included different image processing techniques such as Gabor filters, morphological image processing, Canny's edge detector, least-square fitting interpolation method and geometrical procedures to measure the width.

Recently, Eladawi et al. [31] have introduced an automatic segmentation system for retinal blood vessels from OCTA images. The system was basically based on the Generalized Gauss-Markov random field model and the Markov-Gibbs random field model.

More recently, Tang et al. [32] have presented a novel supervised method based on the Multi-Proportion Channel Ensemble Model to obtain more details on the retinal vessels with reduced computational complexity. The proposed segmentation approach consisted of five identical submodels in order to capture various vessel details once trained on different composition images.

V. Conclusion

In this study, we developed two segmentation and quantification algorithms of CNV on outer retinal flow images acquired with OCT-Angiography, which is a new and very promising non-invasive imaging technique.

These algorithms allow quantifying three biomarkers of neovascular AMD according to the CNV topology. Our segmentation and quantification results, obtained with the automatic algorithms showed a good agreement with the embedded software "AngioAnalytics" measures, calculated after the expert manual delineation of the CNV total area. The proposed methods thus allow automatically obtaining quantitative parameters of the CNV lesion, which can bring a precious aid for clinicians in the follow-up of patients with AMD disease and save time in clinical routine.

For future works, further studies need to be performed in order to overcome the limits of the proposed algorithms and complementary validations have to be carried out to compare our method's accuracy to the embedded software "AngioAnalytics".

References

[1] L. Liu, S. S. Gao, S. T. Bailey, D. Huang, D. Li, and Y. Jia, 'Automated choroidal neovascularization detection algorithm for optical coherence tomography angiography', *Biomedical optics express*, vol. 6, no. 9, pp. 3564–3576, 2015.

[2] X. Wei, D. S. W. Ting, W. Y. Ng, N. Khandelwal, R. Agrawal, and C. M. G. Cheung, 'Choroidal vascularity index: a novel optical coherence tomography based parameter in patients with exudative age-related macular degeneration', *Retina*, vol. 37, no. 6, pp. 1120–1125, 2017.

[3] S. S. Gao *et al.*, 'Quantification of choroidal neovascularization vessel length using optical coherence tomography angiography', *Journal of biomedical optics*, vol. 21, no. 7, p. 076010, 2016.

[4] Y. Jia *et al.*, 'Quantitative optical coherence tomography angiography of choroidal neovascularization in age-related macular degeneration', *Ophthalmology*, vol. 121, no. 7, pp. 1435–1444, 2014.

[5] R. F. Spaide, J. G. Fujimoto, and N. K. Waheed, 'Image artifacts in optical coherence angiography', *Retina (Philadelphia, Pa.)*, vol. 35, no. 11, p. 2163, 2015.

[6] T. E. De Carlo, A. Romano, N. K. Waheed, and J. S. Duker, 'A review of optical coherence tomography angiography (OCTA)', *International journal of retina and vitreous*, vol. 1, no. 1, p. 5, 2015.

[7] A. Camino *et al.*, 'Automated registration and enhanced processing of clinical optical coherence tomography angiography', *Quantitative imaging in medicine and surgery*, vol. 6, no. 4, p. 391, 2016.

[8] A. Baghaie, Z. Yu, and R. M. D'Souza, 'State-of-the-art in retinal optical coherence tomography image analysis', *Quantitative imaging in medicine and surgery*, vol. 5, no. 4, p. 603, 2015.

[9] J. Xue, A. Camino, S. T. Bailey, X. Liu, D. Li, and Y. Jia, 'Automatic quantification of choroidal neovascularization lesion area on OCT angiography based on density cell-like P systems with active membranes', *Biomedical optics express*, vol. 9, no. 7, pp. 3208–3219, 2018.

[10] J. Almotiri, K. Elleithy, and A. Elleithy, 'Retinal vessels segmentation techniques and algorithms: a survey', *Applied Sciences*, vol. 8, no. 2, p. 155, 2018.

[11] M. Bansal and N. Singh, 'Retinal Vessel Segmentation Techniques: A Review', presented at the Proceedings of the World Congress on Engineering and Computer Science, 2017, vol. 1.

[12] Mehta and Kaur, ‘A review on Retinal Blood Vessel Segmentation Techniques’, *International journal for scientific research and development*, vol. 4, no. 6, pp. 1034–1039, 2016.

[13] M. I. Khan, H. Shaikh, A. M. Mansuri, and P. Soni, ‘A review of retinal vessel segmentation techniques and algorithms’, *International Journal of Computer Technology and Applications*, vol. 2, no. 5, pp. 1140–1144, 2011.

[14] K. BahadarKhan, A. A. Khaliq, and M. Shahid, ‘A morphological hessian based approach for retinal blood vessels segmentation and denoising using region based otsu thresholding’, *PloS one*, vol. 11, no. 7, p. e0158996, 2016.

[15] W. S. Oliveira, J. V. Teixeira, T. I. Ren, G. D. Cavalcanti, and J. Sijbers, ‘Unsupervised retinal vessel segmentation using combined filters’, *PloS one*, vol. 11, no. 2, p. e0149943, 2016.

[16] A. F. Frangi, W. J. Niessen, K. L. Vincken, and M. A. Viergever, ‘Multiscale vessel enhancement filtering’, presented at the International conference on medical image computing and computer-assisted intervention, 1998, pp. 130–137.

[17] A. Bird *et al.*, ‘An international classification and grading system for age-related maculopathy and age-related macular degeneration’, *Survey of ophthalmology*, vol. 39, no. 5, pp. 367–374, 1995.

[18] O. Tankyevych, H. Talbot, and P. Dokladal, ‘Curvilinear morpho-Hessian filter’, presented at the 2008 5th IEEE International Symposium on Biomedical Imaging: From Nano to Macro, 2008, pp. 1011–1014.

[19] A. Ali, A. Hussain, and W. M. D. W. Zaki, ‘Segmenting retinal blood vessels with gabor filter and automatic binarization’, *International Journal of Engineering and Technology (UAE)*, vol. 7, no. 4, pp. 163–167, 2018.

[20] M. F. Aslan, M. Ceylan, and A. Durdu, ‘Segmentation of Retinal Blood Vessel Using Gabor Filter and Extreme Learning Machines’, presented at the 2018 International Conference on Artificial Intelligence and Data Processing (IDAP), 2018, pp. 1–5.

[21] N. Memari, A. R. Ramli, M. I. B. Saripan, S. Mashohor, and M. Moghbel, ‘Retinal Blood Vessel Segmentation by Using Matched Filtering and Fuzzy C-means Clustering with Integrated Level Set

Method for Diabetic Retinopathy Assessment', *Journal of Medical and Biological Engineering*, pp. 1–19, 2018.

[22] H. OULHADJ, A. NAKIB, and P. SIARRY, 'Segmentation d'images par maximisation de l'entropie à deux dimensions basée sur le recuit microcanonique', presented at the 21° Colloque GRETSI, Troyes, FRA, 11-14 septembre 2007, 2007.

[23] F. Gargouri, 'Thresholding the maximum entropy', 2012. [Online]. Available: https://fr.mathworks.com/matlabcentral/fileexchange/35158-thresholding-the-maximum-entropy. [Accessed: 15-May-2018].

[24] G. Xiong, 'Fuzzy c-means thresholding'. [Online]. Available: https://fr.mathworks.com/matlabcentral/fileexchange/8351-fuzzy-c-means-thresholding. [Accessed: 29-May-2018].

[25] F. Amoroso, A. Miere, O. Semoun, C. Jung, V. Capuano, and E. H. Souied, 'Optical coherence tomography angiography reproducibility of lesion size measurements in neovascular age-related macular degeneration (AMD)', *British Journal of Ophthalmology*, vol. 102, no. 6, pp. 821–826, 2018.

[26] A. Miere *et al.*, 'Optical Coherence Tomography Angiography to Distinguish Changes of Choroidal Neovascularization after Anti-VEGF Therapy: Monthly Loading Dose versus Pro Re Nata Regimen', *Journal of ophthalmology*, vol. 2018, 2018.

[27] F. Coscas *et al.*, 'Quantitative optical coherence tomography angiography biomarkers for neovascular age-related macular degeneration in remission', *PLOS ONE*, vol. 13, no. 10, p. e0205513, Oct. 2018.

[28] Q. Chen, X. Yu, Z. Sun, and H. Dai, 'The application of OCTA in assessment of anti-VEGF therapy for idiopathic choroidal neovascularization', *Journal of ophthalmology*, vol. 2016, 2016.

[29] D. Xu *et al.*, 'Long-term progression of type 1 neovascularization in age-related macular degeneration using optical coherence tomography angiography', *American journal of ophthalmology*, vol. 187, pp. 10–20, 2018.

[30] F. Oloumi, R. M. Rangayyan, P. Casti, and A. L. Ells, 'Computer-aided diagnosis of plus disease via measurement of vessel thickness in retinal fundus images of preterm infants', *Computers in biology and medicine*, vol. 66, pp. 316–329, 2015.

[31] N. Eladawi *et al.*, 'Automatic blood vessels segmentation based on different retinal maps from OCTA scans', *Computers in biology and medicine*, vol. 89, pp. 150–161, 2017.

[32] P. Tang, Q. Liang, X. Yan, D. Zhang, G. Coppola, and W. Sun, 'Multi-proportion channel ensemble model for retinal vessel segmentation', *Computers in biology and medicine*, vol. 111, p. 103352, 2019.

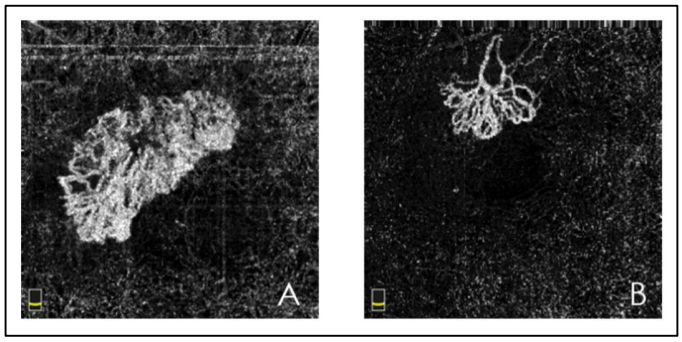

Figure 1: OCTA flow images separation according to the CNV lesion topology. (A): Group 1, densely packed high flow neovascular networks, (B): Group 2, high flow distinguishable neovascular networks.

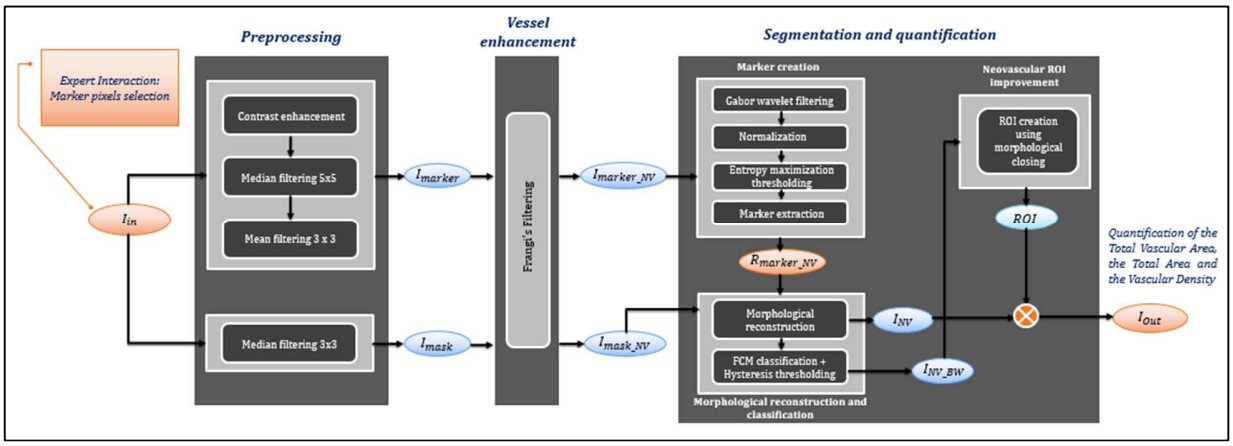

Figure 2: Overview of the developed choroidal neovascularization (CNV) segmentation algorithm for Group 2 flow images. Input image Iin goes through four main steps: "Preprocessing", ensuring noise reduction by classic filtering. "Vessel enhancement" by Frangi filtering. "Segmentation" mainly based on Gabor wavelets, entropy maximization thresholding, morphological reconstruction and Fuzzy-C-Means classification. The final step "Quantification" ensuring the automatic measurement of three biomarkers of neovascular AMD: total vascular area (TVA), total area (TA) and vascular density (VD).

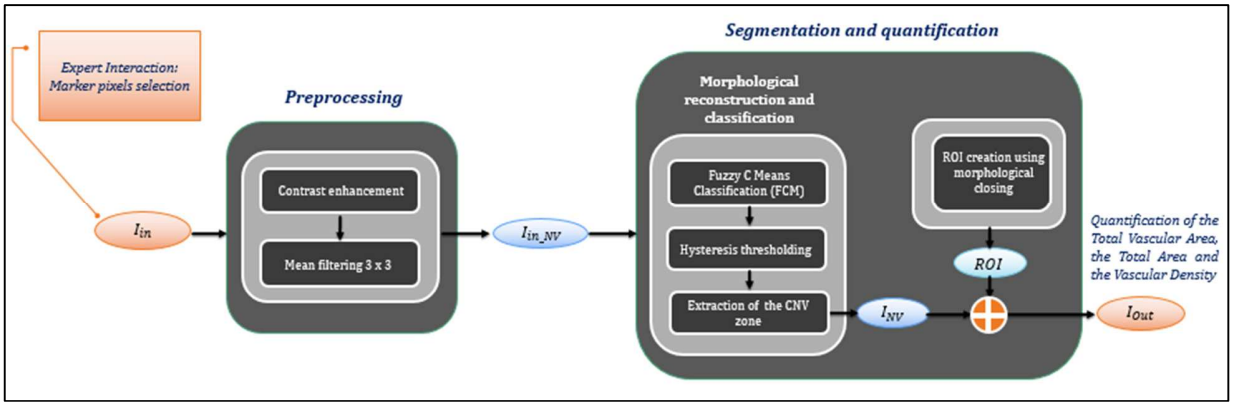

Figure 3: Overview of the developed choroidal neovascularization (CNV) segmentation algorithm for Group 1 flow images. The input image I_{in} goes through three main steps: "Preprocessing" to ensure noise reduction by classic filtering. "Segmentation" mainly based on Fuzzy-C-Means classification and hysteresis thresholding. The final step "Quantification" ensures the automatic measurement of the three biomarkers of neovascular AMD: total vascular area (TVA), total area (TA) and vascular density (VD).

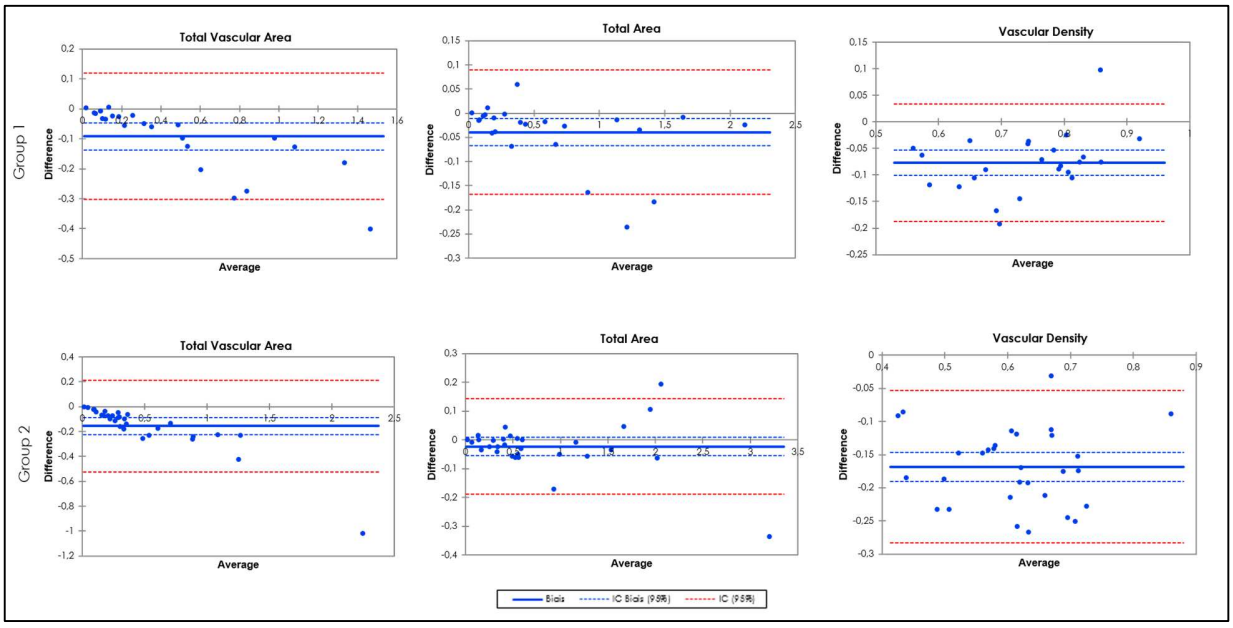

Figure 4: Bland and Altman plots showing the inter-methods agreement for the three biomarkers measurements (TVA, TA and VD).

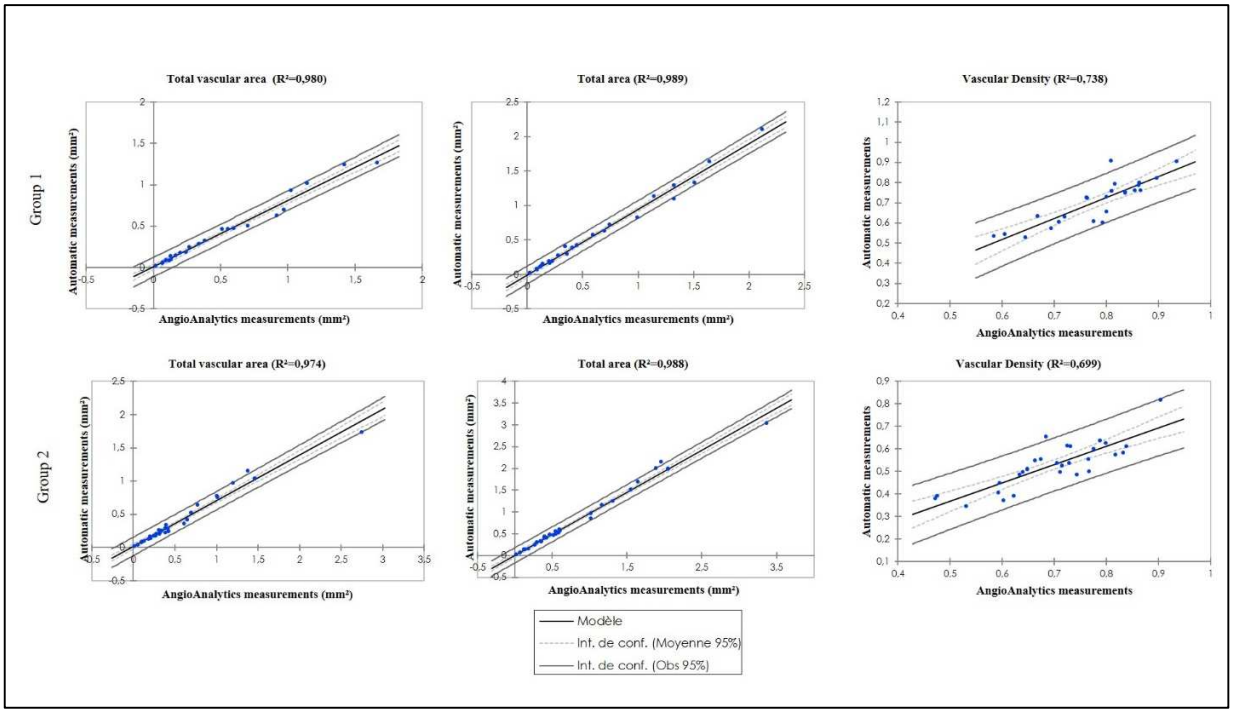

Figure 5: Linear regression plots between the automated and the manual method for the three biomarkers measurements (TVA, TA and VD) in each group.

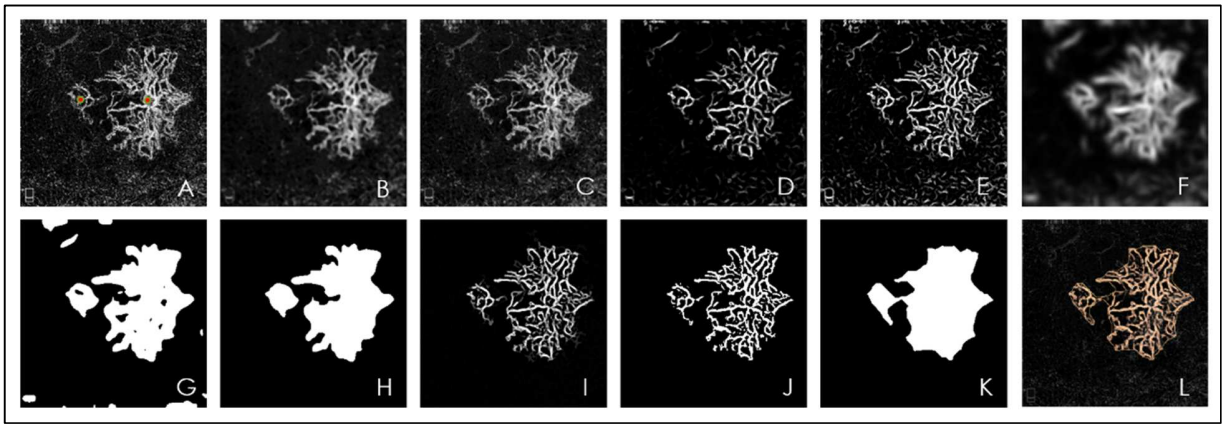

Figure 6: Proposed choroidal neovascularization segmentation algorithm step-by-step results for the Group 2 flow images. (A) Original image, (B) 1st preprocessing, (C) 2nd preprocessing, (D) vessel enhancement using Frangi on (B), (E) vessel enhancement using Frangi on (C), (F) Gabor wavelet filtering on (D), (G) entropy maximization thresholding on (F), (H) neovascular ROI extraction, (I) morphological reconstruction on (E) using (H), (J) hysteresis thresholding on (I), (K) morphological closing on (J) and (L) the segmented CNV.

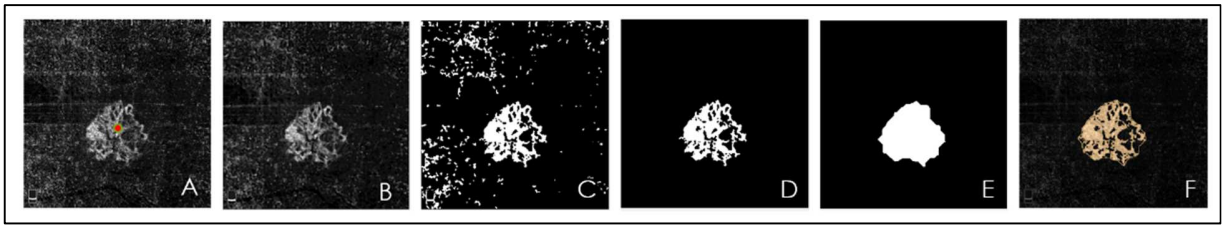

Figure 7: Proposed choroidal neovascularization segmentation algorithm step-by-step results for Group 1 flow images. (A) Original image, (B) preprocessing, (C) hysteresis thresholding, (D) neovascular ROI extraction, (E) morphological closing on (D) and (F) the segmented CNV.

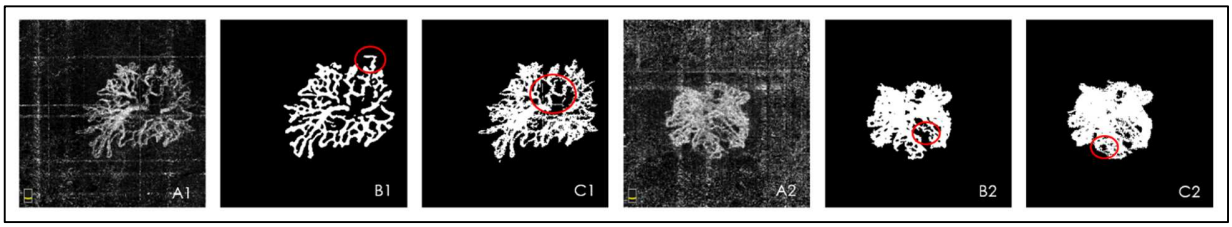

Figure 8: AngioVue segmentations against our proposed segmentations for both groups of flow images. (A1) Original image of Group 2, (B1) our proposed segmentation, (C1) AngioVue segmentation, (A2) original image of Group 1, (B2) our proposed segmentation and (C2) AngioVue segmentation.

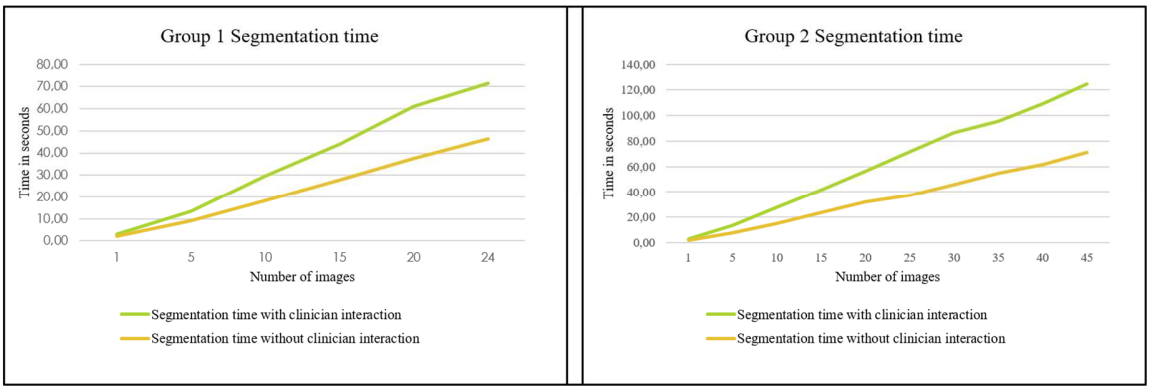

Figure 9: Performance evaluation of the two algorithms on regards to the segmentation time. The segmentation time without clincician interaction is linear and depends only on the machine performances, whereas the segmentation time with clinician interaction depends on the expert that can take less or more time to select the CNV markers.

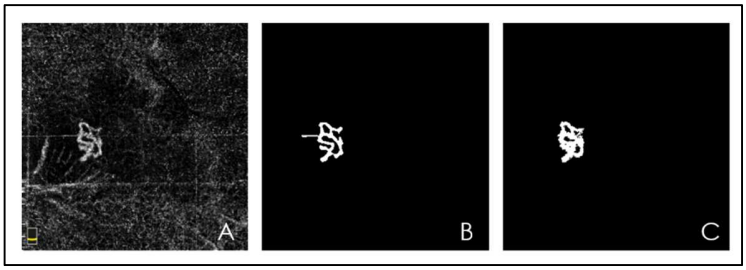

Figure 10: (A) Group 2 original flow image, (B) our proposed automated segmentation where a white line artifact connected to the lesion was segmented as a vascular structure and (C) AngioAnalytics segmentation after manual delineation of the CNV.

		Proposed algorithm	**AngioAnalytics**	**P-value**
Group 1	**TVA**	0.402 ± 0.380 mm^2	0.494 ± 0.469 mm^2	0.00036
	TA	0.592 ± 0.564 mm^2	0.631 ± 0.591 mm^2	0.008
	VD	70.3 % ± 11.0 %	77.9 % ± 9.1 %	< 0.0001
Group 2	**TVA**	0.400 ± 0.395 mm^2	0.556 ± 0.568 mm^2	< 0.0001
	TA	0.791 ± 0.740 mm^2	0.815 ± 0.761 mm^2	0.143
	VD	52.6 % ± 10.2 %	69.4 % ± 10.4 %	< 0.0001

Table 1: Comparision between our automatic quantification results and AngioAnalytics quantification. Mean ± standard deviation of the three biomarkers: Total Vascular Area (TVA), Total Area (TA) and Vascular Density (VD) from the 24 flow images of Group 1 and the 30 flow images of Group 2. P-value based on the Student's t-test.

		Bias	SD	CI (95%)
Group 1	**TVA**	-0.092 mm²	0.107 mm²	]-0.137 mm²; -0.046 mm²[
	TA	-0.039 mm²	0.066 mm²	]-0.067 mm²; 0.011 mm²[
	VD	-7.7 %	5.6 %	]-10.0 %; -5.3 %[
Group 2	**TVA**	-0.156 mm²	0.189 mm²	]-0.227 mm²; -0.085 mm²[
	TA	-0.023 mm²	0.085 mm²	]-0.055 mm²; 0.008 mm²[
	VD	-16.8 %	5.9 %	]-19.0 %; -14.6%[

Table 2: Bland and Altman biases, standard deviation biases and 95% confidence interval of the inter-methods agreement for the three biomarkers of both groups. Total Vascular Area (TVA), Total Area (TA) and Vascular Density (VD).

	Saliency method	DEC P Systems	Our proposed methods
Jaccard coefficient	0.589 ± 0.253	0.872 ± 0.053	0.875 ± 0.055

Table 3: Performance Comparison of Total Area segmentation with respect to other existing methods. Saliency method and DEC P Systems Jaccard coefficients were computed from 22 participants [9] whereas our proposed methods' Jaccard coefficient was calculated from 54 participants.